A Numerical Model of Trade Wind Weather on Oahu

RONALD L. LAVOIE

Environmental Monitoring and Prediction, National Oceanic and Atmospheric Administration, Rockville, Md. 20852

(Manuscript received 9 May 1974, in revised form 28 June 1974)

ABSTRACT

A single-layer mesoscale model, originally developed for the study of wintertime lake-effect storms, is applied to the airflow over the Island of Oahu, Hawaii. Terrain effects, land roughness, island heating, and surface evaporation are all included. Convective precipitation and latent heating are parameterized in terms of larger-scale motions resolved on the 3-km×3-km grid.

Experiments were conducted with an atmospheric structure consistent with typical trade conditions as well as with variations from normal wind speed and inversion height. Satisfactory agreement was achieved with observed patterns of inversion height, cloud base height, temperature, relative humidity, wind flow, and precipitation under typical conditions. Mixing of dry air through the inversion from above was deduced to be very important. In most experiments the model generated a hydraulic jump to the lee of the mountains. Sea breeze effects were only partially simulated. Under some conditions the blocking effect of the Island in the model resulted in less than 40% of the upstream air surmounting the central part of the windward mountain ridge, so that vertical cross-section models are contraindicated.

1. Introduction

Understanding the temporal variations and spatial distributions of weather on mountainous islands in the trade regions offers a great challenge. Rainforests and deserts can be separated by just a few miles. Apparently slight changes in atmospheric structure or wind flow can result in dramatic changes in cloudiness and precipitation.

Weather regimes in the Hawaiian Islands have been studied extensively (Leopold, 1949; Leopold *et al.*, 1951; and others). The critical features determining weather in a locality are the strength and direction of the low-level wind, the topography, the height and intensity of the trade inversion, and the land-sea breeze regime. These local influences are impressed upon synoptically induced weather and usually dominate.

A qualitative understanding of these interactions has been gained over the years, but the local complexities are great and quantitative description is still incomplete. The disturbance in the wind field induced by a mountainous island, the magnitude of the rainshadow effect and the perturbation of the inversion surface are among the several poorly explored questions. Many of these questions can be answered by application of numerical models.

The demands upon numerical modeling in such a problem are severe, however. Irregular shapes and topography require three-dimensionality. Clouds and precipitation must be included. Surface forcing through roughness, terrain, and heating are obviously important. Vertical resolution is required to delineate the inversion and sea breeze circulations. Such a model is within the state of the art, but the computer requirements would preclude broad application or experimentation.

This paper reports the results of applying a simplified mesoscale model to the Island of Oahu. The model was developed to simulate local wintertime storms around the Great Lakes (Lavoie, 1972), but the assumptions involved make it at least as well suited to trade wind conditions. The objective here is not to reproduce all processes occurring in the interaction of an airstream with a tropical island but to contribute to a better understanding of first order effects.

2. The model

Let us try to represent a tradewind sounding by three distinct layers as shown in Fig. 1. The lowermost layer has a superadiabatic lapse rate indicative of surface heating. Most of the wind shear due to surface friction is assumed to be constrained to this lower layer as well. The thickness of the layer is taken to be about 50 m. The middle layer is assumed to be well mixed so as to be essentially homogeneous in its vertical distribution of potential temperature as well as moisture and momentum. The mixed layer is modeled to have a distinct upper boundary, at height h, characterized by an inversion surface or at least a first order discontinuity in lapse rate, separating a deep stratum of relatively stable air aloft.

We shall limit the time-dependent calculations to the middle layer while parameterizing interactions with the surface boundary layer and with the overlying

stable layer. The level h will be identified with the trade wind inversion and has a height of the order of 1 to 3 km. Cumulus clouds will be expected within the mixed layer. Surface forcing will perturb the layer causing accelerations, convergence, changes in temperature and moisture and alterations in the depth of the layer. There are five dependent variables: the two horizontal components of the vector wind, $\mathbf{V}$; the potential temperature of the layer, θ; the specific humidity, q; and the height h representing the top of the mixed layer.

The derivation of the predictive equations for these five variables is given in Lavoie (1972) and will not be repeated here. The equations result from a vertical integration of the basic equations applying to a fluid parcel in the mixed layer. The hydrostatic and incompressibility assumptions are made. The resulting equations are

$$\frac{\partial V}{\partial t}=-\mathbf{V}\cdot\nabla\mathbf{V}-\mathbf{k}\times f\mathbf{V}-\mathbf{F}_i-(h_i-h)f\mathbf{k}\times\frac{\partial \mathbf{V}_g}{\partial Z}+\frac{g}{\theta_h}\left[\theta-\theta_h-\frac{\Gamma}{4}(h_m-h_i)\right]\nabla h+\frac{g}{\theta}(h-Z_s)\nabla\theta-\frac{C_D}{(h-Z_s)}|\mathbf{V}|\mathbf{V} \quad (1)$$

$$\frac{\partial\theta}{\partial t}=-\mathbf{V}\cdot\nabla\theta+\frac{C_D'}{(h-Z_s)}|\mathbf{V}|(\theta_0-\theta)+\frac{L\theta\bar{\alpha}M}{c_p\bar{T}(h-Z_s)} \quad (2)$$

$$\frac{\partial h}{\partial t}=-\mathbf{V}\cdot\nabla h+W_s-(h-Z_s)\nabla\cdot\mathbf{V}+\left(\frac{1}{\Gamma}\frac{\partial\theta}{\partial t}\right)_{\theta=\theta_h} \quad (3)$$

$$\frac{\partial q}{\partial t}=-\mathbf{V}\cdot\nabla q+\frac{C_D''|\mathbf{V}|}{h-Z_s}(q_0-q)-\frac{\beta|W_h|}{h-Z_s}(q-q_h)-\frac{\bar{\alpha}M}{h-Z_s}. \quad (4)$$

The momentum equation (1) includes the nonlinear advective term and the Coriolis force. The third term, $\mathbf{F}_i$, represents the pressure gradient force at the undisturbed height of the inversion surface while the fourth term provides for the contribution of the thermal wind above the inversion resulting from a displacement of the inversion surface. Here h_i is the initial height of the inversion and $\mathbf{V}_g$ is the geostrophic wind in the upper stable layer. The fifth term represents the restoring force set up in the pressure field by a disturbance of the inversion surface; θ_h is the potential temperature at the base of the upper stable layer, g is the local acceleration due to gravity, Γ is the vertical gradient of θ in the stable layer, and h_m is the maximum height of the inversion surface in the computational domain. The sixth term is the contribution to acceleration made by diabatic heating. Horizontal gradients of potential temperature in the mixed layer become equivalent to horizontal pressure gradients because of the hydrostatic assumption. The final term represents the momentum flux through the local boundary parameterized through the use of a drag coefficient, C_D, whose value will differ considerably between land and sea. Subscripts h, s, and 0 refer the variables to levels defined in Fig. 1.

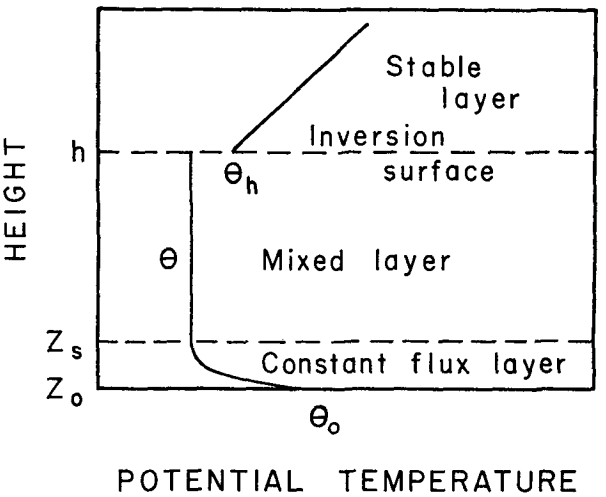

FIG. 1. Thermal structure assumed in the model.

The tendency equation for θ, Eq. (2), includes a parameterization of heat flux from below using the same bulk aerodynamic method used for momentum. Here C_D' is the drag coefficient for heat and θ_0 is the potential temperature of the ground or water surface. The last term of (2) provides for latent heat delivery to the mixed layer at a rate proportional to M, the local rainfall rate, to be discussed shortly. The other quantities in this term have standard notation: L is the latent heat coefficient, c_p is the specific heat at constant pressure, and $\bar{\alpha}$ and $\bar{T}$ are the mean values for the mixed layer of specific volume and temperature respectively.

The tendency equation for the height of the inversion surface (3) results from vertical integration of the continuity equation for an incompressible fluid. The term W_s is the terrain-induced upward motion through the lower boundary of the mixed layer, given by

$$W_s=\mathbf{V}\cdot\nabla Z_0.$$

The next term gives the contribution of vertical motion generated at the inversion surface by divergence within the mixed layer. The final term is included whenever $\theta=\theta_h$, i.e., when the inversion disappears; in this event diabatic heating serves to increase the depth of the mixed layer directly.

The final predictive equation (4) is an expression of moisture conservation. Surface evaporation and upward flux is again parameterized by means of an

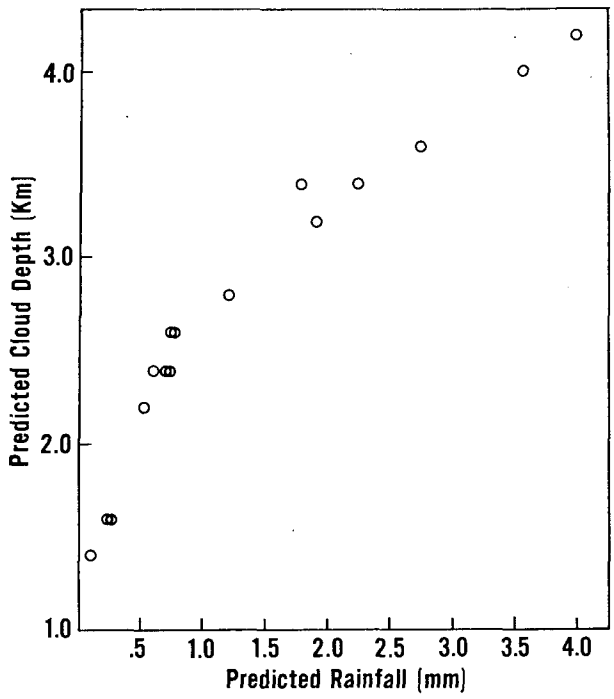

FIG. 2. Rainfall versus cloud depth predicted for 16 trade wind experiments using a one-dimensional cumulus cloud model. From Fields (1971).

appropriate drag coefficient. The last two terms are moisture sinks. One involves an arbitrary attempt to parameterize the downward mixing of dry air through the inversion. It depends upon the difference in specific humidity across the inversion layer and is modulated by the magnitude of the mesoscale vertical velocity (W_h) at that level using an arbitrary coefficient, β. The vertical velocity at an arbitrary height Z is calculated by integrating the divergence upward from the surface through the mixed layer to the level Z, i.e.,

$$W_Z = W_s - (Z - Z_s)\nabla \cdot \mathbf{V}. \tag{5}$$

The last term in (4) reflects the net vapor loss due to the mean rainfall rate M.

3. Parameterization of clouds and precipitation

The question of how to calculate the local rainfall rate remains. The rain will be generated by cumulus clouds that cannot be directly simulated by the model. Nonetheless, the experiments are predicated upon the hypothesis that the location and intensity of the convection will be dictated by the pattern of disturbance on the mesoscale. For example, cloud depth can be expected to depend upon the lifting condensation level and upon the height of the inversion, and it is well known that depth is a major determinant of rain potential from a cumulus cloud.

Some guidance on how rainfall varies with cloud depth is available from experiments with numerical models of cumulus clouds. Figure 2 shows results of such a study by Fields (1971) using the Pennsylvania State University cumulus model. This is a one-dimensional Lagrangian model which makes use of a bulk entrainment law. Condensed water is partitioned into cloud droplets and raindrops with parameterized rates of transfer between these two classes. The active cloud updraft is relieved of that fraction of rainwater (in a Marshall-Palmer size distribution) whose terminal fall speed exceeds the updraft speed. When the lead cloud parcel reaches its maximum altitude, all rainwater dropped out during the ascent of the parcel is taken together with the rainwater content of all other parcels in the steady-state cloud to determine the total rainfall generated by the cloud.

The parameters in Fields' version of the model had been tuned so that model predictions of cloud top and liquid water content agreed very well with cloud structure observed during a field program in St. Croix, U. S. Virgin Islands. Rainfall predictions could not be verified directly, but there was qualitative agreement with radar observations. Figure 2 shows predictions of rain amount versus cloud depth for 16 simulations of individual clouds near St. Croix. It is seen that the model cloud must be deeper than 1 km before significant rain is produced. At first the rain amount increases slowly with cloud depth, but the rain production becomes more and more efficient the deeper the cloud. The model utilized for Fig. 2 is a great oversimplification, but it provides a starting point for a parameterization scheme.

Using typical durations and areal coverage of showers, the curve in Fig. 2 can be used to estimate the average rain rate over a representative area due to contributions of many cumulus clouds. For example, experience in St. Croix showed that a field of maritime cumulus with depths of 3 km could be expected to produce echoes with durations of about 12 min and areal coverage on a PPI scope of about 5%. Taken together with the data in Fig. 2, these parameters lead to a mean-area rainfall rate of about 0.4 mm hr^{-1}. A few such values were calculated for different cloud depths and were fitted by a parabolic relationship, as shown in Fig. 3, between cloud depth, D, and mean rain rate, N.

Now the curve is meant to apply to relatively undisturbed conditions. An important modulating factor is felt to be moisture flux convergence in the subcloud layer, so that the final form of the relationship for M,

$$M = (\epsilon W_{cB} + 1)N \text{ cm hr}^{-1}, \tag{6}$$

includes a multiplier involving the mesoscale vertical velocity at cloud base, W_{cB}, in units of cm sec^{-1}. W_{cB} is calculated from (5). The coefficients are selected in such a way that subsidence of 2 cm sec^{-1} is sufficient to suppress convective precipitation (i.e., $\epsilon = 0.5$ sec cm^{-1}), while positive values of W_{cB} increase the precipitation rate in proportion to the upward motion. When

M becomes negative, it is set to zero. Except for the form of N, this is the same expression used earlier in the case of lake-effect storms.

The cloud depth, D, is taken to be the height difference between the lifting condensation level (LCL) of a parcel at the base of the mixed layer and the height of the base of the inversion at that point. The LCL can be readily calculated from local values of θ and q by standard techniques (e.g., Petterssen, 1956).

With a relationship available for the calculation of M from predicted mesoscale quantities, the prognostic equation set is complete. The system of equations can be solved numerically as an initial value problem with appropriate boundary conditions.

4. Experimental design

A 3 km×3 km grid mesh of 2000 points was used for numerical representation of the variables over the Island and nearby ocean. The grid separation increased exponentially away from the Island so as to effectively isolate the domain boundaries. Figure 4 shows the grid mesh in the vicinity of Oahu as well as the Island topography as analyzed from the somewhat smoothed values assigned to the grid points. The smoothing was accomplished by use of a moving 9-point weighting operator represented by the matrix

$$\left|\tfrac{1}{4}\ \tfrac{1}{2}\ \tfrac{1}{4}\right| \cdot \begin{pmatrix} \tfrac{1}{4} \\ \tfrac{1}{2} \\ \tfrac{1}{4} \end{pmatrix}.$$

Its filtering properties are such that wavelengths of two grid increments are completely suppressed, but the damping decreases with increasing wavelength. Two-grid increment forcing is known to give rise to nonlinear instability in numerical calculations. In order to recover much of the topography at other wavelengths, however, a "desmoothing" was accomplished using the weighting operator,

$$\left|\tfrac{1}{4}\ -\tfrac{3}{2}\ \tfrac{1}{4}\right| \cdot \begin{pmatrix} \tfrac{1}{4} \\ -\tfrac{3}{2} \\ \tfrac{1}{4} \end{pmatrix},$$

yielding the grid point values analyzed in Fig. 4. The resulting topography is intended to be compatible with the 3-km grid mesh and does not fully reflect local extremes. For example the maximum model terrain height is 740 m on the western ridge while the actual summit elevation there exceeds 1100 m.

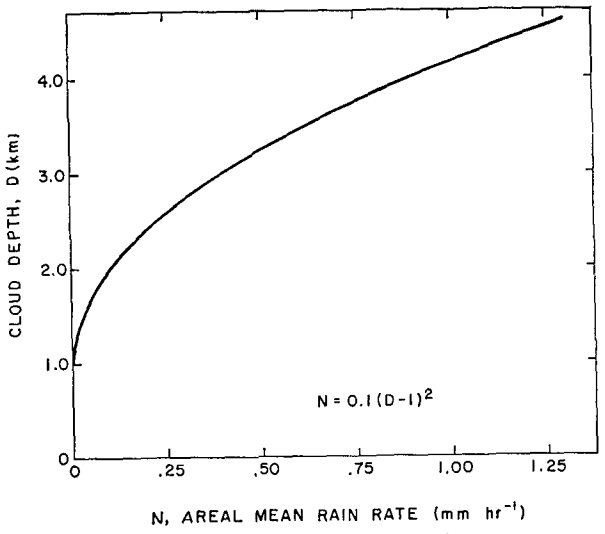

FIG. 3. Parameterized relationship between maximum cloud depth and mean rain rate in the absence of mesoscale convergence.

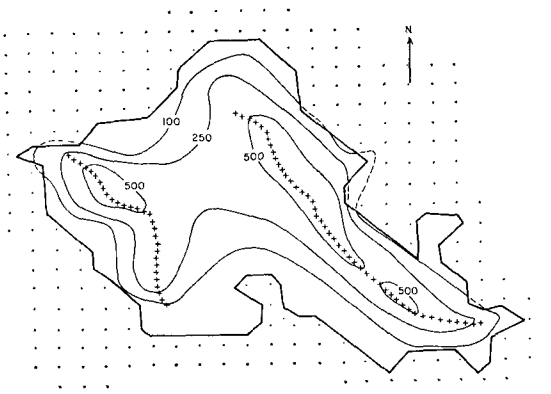

FIG. 4. Representation of Oahu used in the model experiments. Smoothed topography (in meters) and representative grid point mesh are shown.

The initial meteorological conditions are selected so as to provide balanced flow with respect to the open ocean at all grid points. At time $t=0$, the Island "springs up" with its heat and moisture source, its roughness differential and its topography. The readjustment process is followed at each grid point by means of Eqs. (1) through (4) expressed in finite difference form using the forward-upstream scheme described by Lavoie (1968) and used earlier by Estoque (1962) and Orville (1965) among others. A time step of 100 sec was used to advance the dependent variables. The integration was continued until the rate of change of the variables became sufficiently small in the region of interest to assure a near steady-state solution. This usually required less than 2.5 hr of meteorological time and about 280 sec of computer time on an IBM 360–67.

During the course of the integration, the dependent variables were held constant at the inflow boundaries. These are sufficiently far upstream from the disturbance so that constancy is a very good approximation. At the outflow boundaries the values of the dependent variables were set equal, at each time step, to the values at the next grid point upstream.

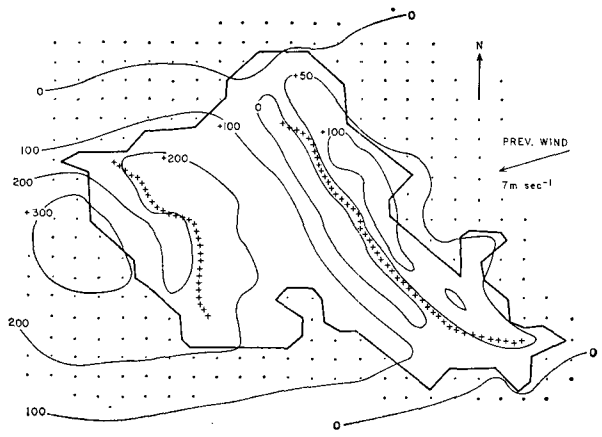

5. Steady FIG.-state solution of inversion perturbation from mean state, in meters.

The following values of parameters were specified for all experiments.

$$C_D = 1.5\times10^{-3} \text{ [ocean]}$$
$$= 7.0\times10^{-3} \text{ [land]}$$
$$C_D' = 7.0\times10^{-3} \text{ [land]}$$
$$= 0 \text{ [}\theta \geq \theta_o \text{ or ocean]}$$
$$C_D'' = 2.1\times10^{-3} \text{ [land]}$$
$$= 0 \text{ [ocean or cloud base} = Z_s\text{]}$$
$$f = 5.25\times10^{-5} \text{ sec}^{-1}$$
$$\beta = 1.25$$

The drag coefficient values for momentum and heat are those used in experiments with Lake Erie (Lavoie, 1972). The coefficient for moisture flux, C_D'', is 30% of the value of the other coefficients over the land surface. This latter choice amounts to setting the average evaporation rate to 30% of the potential evapotranspiration rate for that surface at that temperature. Since the prevailing flow is assumed to be essentially at equilibrium with respect to the ocean, no heat or moisture flux is allowed across the sea surface. The value of the coefficient β was initially set arbitrarily to unity and adjusted upward slightly by trial and error.

5. Simulation of typical trade conditions

The most representative condition for Oahu weather is also the average, at least during the early summer when the trades are most persistent. Furthermore, the precipitation patterns are especially well documented for these conditions.

Typical daytime values of atmospheric structure for the summer months were selected to test the ability of the model to simulate typical Oahu weather. The following "undisturbed" values were used.

$$\left.\begin{aligned} v &= 1.9 \text{ m sec}^{-1} \\ u &= -6.8 \text{ m sec}^{-1} \end{aligned}\right\} \text{ i.e. } \begin{aligned} &\text{speed: } 7.0 \text{ m sec}^{-1} \\ &\text{direction: } 75° \end{aligned}$$

$$\theta_0 = \theta = 297\text{K [ocean and air temperature]}$$
$$\theta_h = 300.5\text{K [i.e., inversion intensity of 3.5K]}$$
$$\theta_L = 303\text{K [heated land temperature]}$$
$$h_i = 2.2 \text{ km}$$
$$\Gamma = 3.0\text{K km}^{-1}$$
$$q = 13.5 \text{ g km}^{-1}$$
$$q_h = 5 \text{ g kg}^{-1}$$
$$\frac{\partial v_g}{\partial Z} = 1.1 \text{ m sec}^{-1} \text{ km}^{-1}$$
$$\frac{\partial u_g}{\partial Z} = 4.1 \text{ m sec}^{-1} \text{ km}^{-1}$$

These values were selected mainly on the basis of data from Mordy and Eber (1954) and Lavoie (1967a). For these conditions the relative humidity at the 1000-mb level is about 71% and cloud base is calculated in the model to be 670 m. When Eq. (2) is applied over land, θ_L is substituted for θ_0; the land-ocean temperature contrast of 6K is judged to be representative of mid-day conditions.

Figure 5 shows the inversion deformation predicted by the model after steady state is achieved under the above conditions. The windward mountain barrier (the Koolau Range) causes the inversion to be lifted a maximum of about 150 m. The air at the top of the mixed layer begins to descend even before reaching the crest, drops to minimum heights just beyond the ridge, then rises abruptly in a mild hydraulic jump. The inversion deformation is greater over the leeward ridge (the Waianae Range) and the highest inversion heights are found just off the leeward coast. The elevated inversion extends many tens of kilometers downwind of the Island. Slight subsidence of the inversion occurs north and south of the Island barrier.

Few data are available on inversion deformation. Some information can be deduced from a diagram presented by Mordy and Eber (1954) based on ten days of aircraft measurements over the Koolaus in the month of June. Their "typical cross section" shows a lifting of the inversion by about 700 ft (213 m) reaching a maximum approximately 4 km upwind of the ridge. From this point the inversion was shown to dip rapidly to an altitude slightly below the undisturbed height upwind of the island. Conditions were not depicted farther downwind or over the Waianaes.

Figure 6 shows the cloud base height calculated by the model using the lifting condensation level (LCL) of air at the bottom of the mixed layer. The Island brings about a net drying of the subcloud layer as a result of rainout of moisture and mixing down of very dry air aloft. This, together with the heating of the air, causes cloud bases to rise to over 1100 m at the leeward coast. Relative humidity (at 1000 mb) is shown at selected points; values decrease from 71% to 54% during the passage of the air across the Island. Temperature increased by 1.0C from windward to leeward shores.

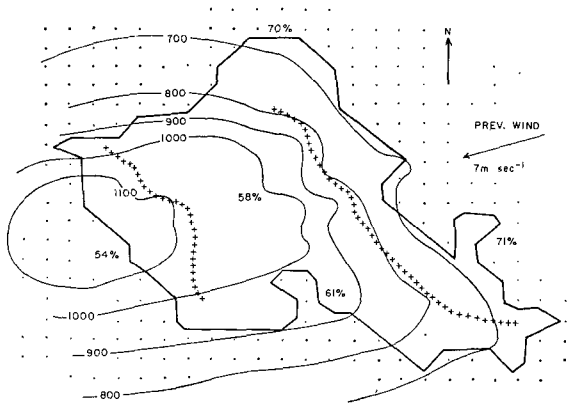

FIG. 6. Predicted cloud base height distribution, in meters. Selected values of surface relative humidity are indicated.

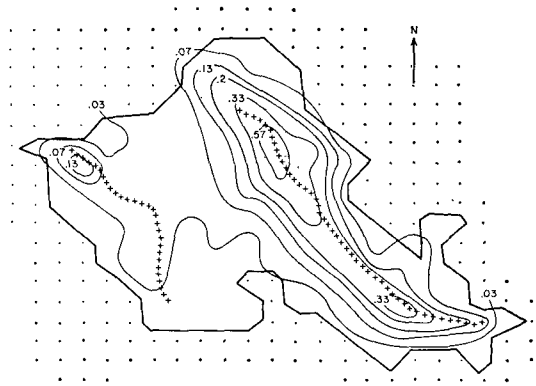

FIG. 8. Observed mean rain rate, June and July, in inches per day. From PRI-HSPA (1955).

Systematic surveys of cloud base height variations are not available, but the pattern shown is qualitatively correct. The summit of Mt. Kaala at 1100 m in the Waianaes is frequently visible below cloud base under typical trade conditions. The aircraft observations of Mordy and Eber referred to earlier show a lifting of cloud base by over 400 m as the air crosses the Koolaus. The decrease in humidity across the Island is also commonly observed. It is one of the features contributing to the greater comfort level generally attributed to the leeward coast.

Rainfall is probably the most easily and thoroughly measured variable available to us. Figure 7 shows the model *prediction* of rainrate in inches day^{-1}. Rainfall is concentrated over the two ridges, with maximum values found just to the lee of the crests. Amounts are much lower in the Waianaes, in spite of the higher terrain, because the higher cloud bases result in decreased cloud depths.

The rainfall rate is calculated from Eq. (6), but this quantity is meant to represent the mean rain production rate within the cloud layer. Wind transport of the raindrops must be accounted for in order to relate to surface precipitation measurements, and this has been done in arriving at the pattern in Fig. 7. A simple constant displacement of 3.5 km in the direction of the mean wind was applied to represent a mean settling speed of 2 m sec^{-1} for the rain through an average depth of fall of 1000 m within a horizontal airflow of 7 m sec^{-1}.

The values and patterns of Fig. 7 can be compared with *observed* averaged daily rainrates for the months of June and July shown in Fig. 8 (from PRI-HSPA, 1955). The location of maxima correspond quite well although the observed amounts are somewhat less than predicted, especially over the Waianaes. One factor contributing to this could be the neglect of evaporation of rain below cloud base. Also it must be remembered that the experiments include daytime heating. If the calculations are redone without land-sea temperature contrast, the rainfall predictions are altered to those found in Fig. 9. There is only a very slight decrease in rain amounts over the Koolaus, but a drastic reduction takes place over the Waianae's. The average of the day and night predictions would show excellent agreement with observed mean rainfall, although the agreement is probably fortuitous. Examination of hourly rainfall data for several summer months for gauges in

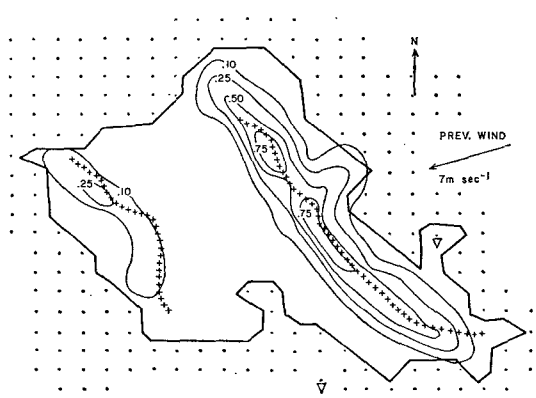

FIG. 7. Predicted rain rate in inches per day. Shower symbols indicate trace amounts.

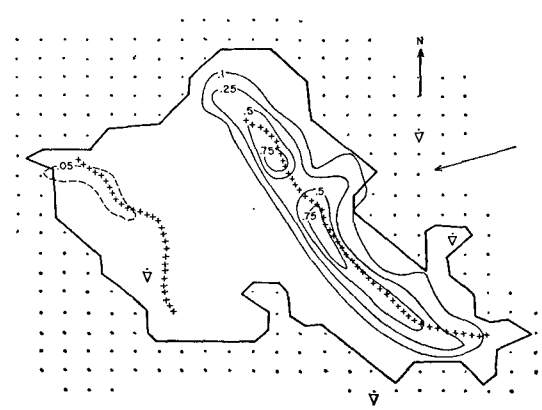

FIG. 9. Same as Fig. 7 except without Island heating.

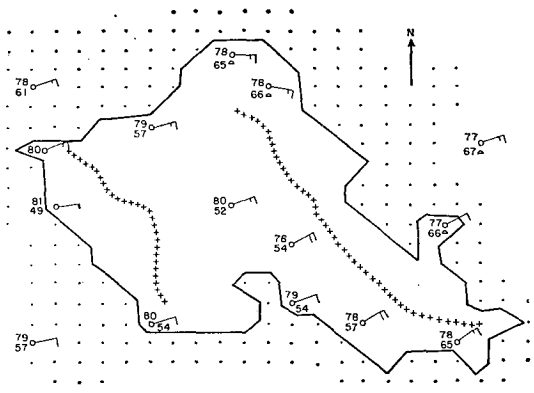

FIG. 10. Weather representation from model results at selected grid points. Each half wind barb represents 5 m sec^{-1}, upper number is surface temperature, and lower number is dew point.

the Waianae region do not reveal a pronounced diurnal variation except on the lee shore which has a strong midday rainfall maximum. Over the ridge there was a tendency for late afternoon and early evening maxima. Farther east the peak rainfall appeared to be during the nighttime hours.

The mean layer airflow diverges somewhat around the Island barrier. For these typical trade conditions the disturbed winds in the model results show a 16° difference in direction across the length of the Island normal to the airstream. Mass flux calculations reveal that 87% of the upwind mass surmounts the Koolau Range; the remainder is forced around the perimeter of the Island and converges to its lee. The wind speeds are enhanced by 3 m sec^{-1} to 4 m sec^{-1} over the mountain ridges compared to the upstream value.

6. Other experiments

As illustration of a more extreme interaction between airstream and Island, we might examine the results of lowering the height of the inversion to 1.1 km. All other parameters and variables were unchanged from the previous experiment. Because the mixed layer barely surmounts the ridge crests in this case, the barrier effect should be severe.

Some of the model results for this experiment are shown in Fig. 10 by means of suitably chosen "observing stations." There was no precipitation anywhere; in fact, except for the windward coast, the Island and its immediate vicinity downwind was predicted to be clear (the LCL was higher than the inversion).

With a lower inversion the wind disturbance was greater than in the typical trade case. There was a directional shift of about 45° across the length of the Island. The maximum wind speed was 10.3 m sec^{-1} to the lee of the Koolaus, the minimum was about 3 m sec^{-1} on the western coast.

The drying effect of the Island was accentuated with a lower inversion, in spite of the lack of rainfall. The drying was due entirely to mixing across the inversion which was quite pronounced because of a strong hydraulic jump to the lee of the Koolaus. In this region the inversion surface rose over 400 m in less than 6 km. Since mixing was parameterized to be proportional to the slope of the inversion, entrainment of dry air would be quite vigorous in this region.

As might be expected with a shallow mixed layer, the Island acts as an effective barrier to the flow. Only 60% of the air immediately upwind of the Koolau range passes over the barrier. Near the center of the ridge the flux is only 39% of that upwind. The numbers give some indication of the degree of error to be expected from the application of two-dimensional vertical cross-section models that require the assumption of non-divergence normal to the cross section.

A limited number of experiments with other initial conditions indicate that, e.g., stronger inversions result in a reduced island disturbance and relatively more reduction of precipitation over the Koolau ridge than elsewhere. Weaker winds have somewhat the same effect although the rainfall now actually increases slightly over the Waianaes as heating effects begin to dominate over topography.

With a wind speed increase to 11 m sec^{-1} and otherwise typical trade conditions, the inversion disturbance is greatly enhanced, leading to nearly twice as much rain over the Koolaus. However, because of the resulting increase in the parameterized mixing across the inversion, there is extreme drying downwind of the Koolaus and no rainfall over the Waianaes.

7. Discussion and conclusions

A single-layer model is seen to be capable of a rather realistic simulation of some aspects of island-induced weather in the trades. The model has many limitations worth discussing, but the assumption of vertical homogeneity is the most severe. Because of that limitation, for example, no sea breeze circulation can develop within the mixed layer in response to island heating. The consequence of daytime heating in the model is indeed to create convergence over the Island as would be expected in the lower levels from a sea breeze circulation. However, all compensating divergence must occur above the inversion, contrary to observation (Lavoie, 1967b).

Oahu is known to rarely support a strong sea breeze (Leopold, 1949), and the above limitation may be relatively unimportant in this case. Nonetheless, it seems unlikely that the model could be used to simulate diurnal rainfall variations, for example. In general one would expect this model to apply best to a small mountainous island under at least moderate wind speeds and/or weak surface heating. The prevailing flow of course should be characterized by a well mixed layer surmounted by a distinct stable layer.

Other model limitations involve questionable, or at least poorly substantiated, forms of parameterization for the pressure gradient disturbance in the upper stable layer, for the entrainment of moisture through the inversion layer, and for convective precipitation. These formulations are exploratory efforts to develop a useful understanding of the role of these phenomena.

For example, the experiments suggest that the loss of moisture in the mixed layer by net entrainment across the inversion is a real and important phenomenon, even though the parameterization used in the current model may be poorly formulated. The "rainshadow" effect proves to be completely incapable of explaining the much reduced rainfall observed over the downwind Waianae range of Oahu. Likewise the observed lifting of cloud base and humidity reduction cannot be explained by surface heating and rainout alone. Mixing across the inversion must be significant, even on the short time scale of cross-island flow.

Another feature of the experiments was the prominence of a hydraulic jump to the lee of both mountain ranges under typical meteorological conditions. These conditions can be predicted for the two-dimensional shallow water equations from standard theory (see, e.g., Houghton and Kasahara, 1968). The modified criteria for three-dimensional barriers with the equation set employed here were investigated by Spellman (1969). Strong winds coupled with a relatively low-level and moderately intense inversion favor the hydraulic jump. The existence of hydraulic jump-like behavior has not been documented over Oahu, but the dissipating clouds to the lee of the Koolaus frequently appear very turbulent both visually and when studied by means of time-lapse photography. Furthermore, very strong gusty winds are often observed on the lee slopes as would be expected in connection with a hydraulic jump.

Because of its relatively modest computational requirements, the model described here is an attractive experimental vehicle. Its generality could be greatly enhanced by addition of one or two layers for improved vertical resolution and by refinements in the parameterization techniques.

Acknowledgments. Most of the research leading to this paper was accomplished while the author was on the faculty of the Pennsylvania State University. Partial support was made available under Grant GA-13818 from the National Science Foundation.

REFERENCES

Estoque, M. A., 1962: The sea breeze as a function of the prevailing synoptic situation. *J. Atmos. Sci.*, **19**, 244–250.

Fields, R., 1971: Modification and testing of a steady-state cumulus model. M.S. Thesis, The Pennsylvania State University, 94 pp.

Houghton, D., and A. Kasahara, 1968: Nonlinear shallow flow over an isolated ridge. *Comm. Pure and Appl. Math.*, **21**, 1–23.

Lavoie, R. L., 1967a: Background data for the warm rain project. *Tellus*, **19**, 348–353.

——, 1967b: Air motions over the windward coast of the Island of Hawaii. *Tellus*, **19**, 354–358.

——, 1968: A mesoscale numerical model and lake-effect storms. Ph.D. dissertation, The Pennsylvania State University, 102 pp.

——, 1972: A mesoscale numerical model of lake-effect storms. *J. Atmos. Sci.*, **29**, 1025–1040.

Leopold, L. B., 1949: The interaction of trade wind and sea breeze, Hawaii. *J. Meteor.*, **6**, 312–320.

——, H. Landsberg, C. K. Stidd, T. C. Yeh, C. C. Wallen, J. E. Carson, and J. J. Marciano, 1951: A group of papers: On the rainfall of Hawaii. Vol. 1, No. 3, *Meteor. Monogr.*, Amer. Meteor. Soc., Boston, 55 pp.

Mordy, W. A., and L. E. Eber, 1954: Observations of rainfall from warm clouds. *Quart. J. Roy. Meteor. Soc.*, **80**, 48–57.

Orville, H. D., 1965: A numerical study of the initiation of cumulus clouds over mountainous terrain. *J. Atmos. Sci.*, **22**, 684–699.

Petterssen, S., 1956: *Weather Analysis and Forecasting*, Vol. 2. New York, McGraw-Hill, p. 42.

Pineapple Research Institute and Hawaiian Sugar Planters Association, 1955: Average Monthly Rainfall Maps. 12 pp.

Spellman, M. J., 1969: Response of the atmosphere to the surface features of a tropical island. M.S. thesis, The Pennsylvania State University, 62 pp.